*Nano Research* 2015, 8(9): 2988–2997
DOI 10.1007/s12274-015-0804-0
**Research Article**
ISSN 1998-0124
CN 11-5974/O4

# Defect- and dopant-controlled carbon nanotubes fabricated by self-assembly of graphene nanoribbons

Cun Zhang and Shaohua Chen (✉)

*LNM, Institute of Mechanics, Chinese Academy of Sciences, Beijing 100190, China*

**Received:** 9 February 2015
**Revised:** 16 April 2015
**Accepted:** 24 April 2015



**KEYWORDS**
graphene nanoribbon,
carbon nanotube,
defect,
dopant,
self-assembly,
molecular dynamics

## ABSTRACT

Molecular dynamics simulations showed that a basal carbon nanotube can activate and guide the fabrication of single-walled carbon nanotubes (CNTs) on its internal surface by self-assembly of edge-unpassivated graphene nanoribbons with defects. Furthermore, the distribution of defects on self-assembled CNTs is controllable. The system temperature and defect fraction are two main factors that influence the success of self-assembly. Due to possible joint flaws formed at the boundaries under a relatively high constant temperature, a technique based on increasing the temperature is adopted. Self-assembly is always successful for graphene nanoribbons with relatively small defect fractions, while it will fail in cases with relatively large ones. Similar to the self-assembly of graphene nanoribbons with defects, graphene nanoribbons with different types of dopants can also be self-assembled into carbon nanotubes. The finding provides a possible fabrication technique not only for carbon nanotubes with metallic or semi-conductive properties but also for carbon nanotubes with electromagnetic induction characteristics.

## 1 Introduction

Defects in carbon nanotubes (CNTs) can change the physical and chemical properties of CNTs through tuning the types, locations, and concentrations of defects [1–6]. For example, vacancy defects in CNTs have high reactivities for physisorption and chemisorption [7]. Stone-Wales (SW) defects can alter the band gap of CNTs [8] and produce valley-valve effects in CNTs [9]. CNTs doped with either boron (B) or nitrogen (N) atoms tend to exhibit metallic behavior [10, 11], whereas CNTs doped with both B and N atoms will possess semiconductive properties [12]. Carbon-boron nitride hetero-nanotubes produced by spiral carbon strips and spiral boron nitride strips can exhibit attractive electronic transport properties, which can be tuned by the chiralities, diameters, and component proportions of the tube and the manner of connection between two strips [13]. Du et al. [14] found that $C_{0.5}(BN)_{0.5}$ single-walled armchair nanotubes could be regarded as gapless semiconductors, independent of tube diameter. It is obvious that the distribution of

Address correspondence to chenshaohua72@hotmail.com

defects or dopants in CNTs should be controlled in order to achieve the desired physical or chemical properties.

To introduce defects or dopants in CNTs, several methods have been suggested according to our knowledge so far: (i) Heteroatoms are directly doped into CNTs during the synthesis of CNTs [10–12, 15–18]; (ii) heteroatoms and functional groups are doped into prepared carbon nanotubes through substitution reactions [19–24]; and (3) vacancies can be induced by high-energetic atom/ion bombardment, and desired dopants can then be filled in [7, 25]. Only the last technique can produce defects in a controllable way with the help of scanning transmission electron microscopy (STEM), which is of course very difficult and complex [7, 25]. Furthermore, it is not practical if one plans to produce a series of defects or dopants with regular distributions in quasi-one dimensional CNTs. How to introduce defects or dopants into CNTs in a controllable way is still an open question since the size of quasi-one dimensional CNTs is extremely small. As a result, the development of CNT-based nano-electronics is unavoidably hindered.

Fortunately, both a recent experiment [26] and a numerical calculation [27] show that single-walled carbon nanotubes can be achieved by self-assembly of graphene nanoribbons (GNRs). The chirality of the self-assembled CNTs can be further predicted according to the width of the GNRs and the radius of a basal CNT. In addition, it is much easier to introduce defects and dopants in quasi-two dimensional GNRs than CNTs because the introduction of defects and dopants into graphene sheets is now controllable [7, 28–34], and great progress has been made in the way of tailoring GNRs with desired shapes and sizes from graphene sheets [35–44]. In view of this progress, an obvious question is whether it is possible to fabricate defect- or dopant-controlled CNTs from the self-assembly of defect- or dopant-predefined GNRs. What is the effect of defect distributions and fractions on the self-assembly of GNRs?

A reactive molecular dynamics simulation was carried out in this study in order to answer these questions. The self-assembly of defect- or dopant-controlled GNRs in a basal CNT was investigated, in which the effects of the types, distributions, and fractions of defects and dopants of different elements as well as the system temperature are considered.

## 2 Computational method

A schematic of the atomistic model is shown in Fig. 1, where a zigzag GNR is inserted into a basal CNT with a depth of 3.0 nm in the axial direction. The basal CNT is fixed and has a chirality of (18,18) and a radius of 1.219 nm. The total length and width of the GNR are 30.09 and 1.77 nm, respectively. Two types of defects and two kinds of dopants in GNRs are considered, including vacancy defects, SW defects, boron dopants, and nitrogen dopants, which are distributed arbitrarily or regularly in the GNRs.

The adaptive intermolecular reactive empirical bond order potential (AIREBO) was adopted in our simulation to describe C–C interactions in GNRs [45]. The Tersoff potential was used for interactions between C–B, C–N, and B–N [46]. Interactions between GNRs and the basal CNT were represented by the commonly used Lennard-Jones (LJ) potential, i.e., $V = 4\varepsilon[(\sigma/r)^{12} - (\sigma/r)^{6}]$, with $\varepsilon_{C-C} = 2.84$ meV, $\varepsilon_{B-C} = 3.294$ meV, $\varepsilon_{C-N} = 4.068$ meV, and $\sigma_{C-C} = 0.34$ nm, $\sigma_{B-C} = 0.34109$ nm, $\sigma_{C-N} = 0.3367$ nm [45, 47, 48].

Both the AIREBO potential and the Tersoff potential are three-body potentials. Nonphysical results may be yielded if the boron or nitrogen fraction in GNRs is relatively large, leading to possible coupling interactions of two kinds of potentials acting on a single atom. As a result, in the present numerical calculations, the fractions of the boron and nitrogen dopants were not larger than 9.0 at.% (percent of atoms) in the GNRs.

All simulations were performed using LAMMPS [49] with a Nosé-Hoover thermostat [50]. The time step was 0.5 fs, and snapshots were recorded every 1.0 ps, which were analyzed by the VMD visualization package [51]. Following our former work [27], in which

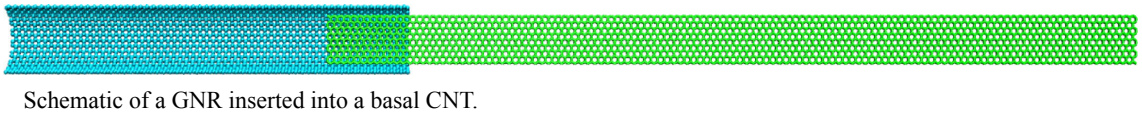

**Figure 1** Schematic of a GNR inserted into a basal CNT.

chirality-controlled CNTs fabricated by self-assembly of GNRs were studied, we adopted the technique of increasing the temperature directly in the present study in order to reduce possible flaws emerging at joint boundaries during the process of self-assembly at a relatively high temperature. Thus, unless otherwise specified in the present work, the temperature remained at 10 K initially for a sufficiently long time to achieve equilibrium, after which the temperature was increased from 10 to 300 K within 1.0 ns and then maintained at 300 K to the end.

## 3 Results and discussion

### 3.1 Self-assembly of perfect GNRs

A perfect GNR inside a basal CNT was investigated first in order to check whether self-assembled CNTs can spontaneously form, though perfect GNRs outside a basal CNT were studied in our former work [27]. The corresponding result is shown in Fig. 2. The initial state of a perfect GNR close to a basal CNT with an insertion length of 3.0 nm is shown in Fig. 2(a). Due to the van der Waals (vdW) attraction between the GNR and the basal CNT, the inserting end of GNRs will spontaneously adhere to the internal surface of the basal CNT and then move forward into the basal nanotube, a snapshot of which is exhibited in Fig. 2(b). Once the left end of the GNRs reaches the left end of the basal CNT, the GNRs will return and twist themselves inside the basal CNT, forming the helical structures shown in Fig. 2(c). Continuous oscillations of the helical structure induce possible collisions between neighboring boundaries, leading to bond formation and the transformation of the helical structures into CNTs, as shown in Fig. 2(d). All the phenomena are consistent with cases of self-assembly of GNRs outside a basal CNT, which have been studied experimentally [26, 52] and numerically [27].

Further geometrical analysis showed that the chirality of the final self-assembled CNT should be (17,9), which agrees well with our theoretical prediction [27], $m = \left\lfloor 2W/\sqrt{3}a + 0.5 \right\rfloor$, $n = \left\lfloor (\sqrt{3(4\pi^2(R-\sigma_{C-C})^2 - W^2)} - W)/\sqrt{3}a + 0.5 \right\rfloor$. Here, $(m,n)$ denotes the chirality of the self-assembled CNT, and $W$ and $a$ are the width of GNRs and the radius of the basal CNT, respectively. Here, $W$ is 1.77 nm, $a$ is 1.219 nm, and $\sigma_{C-C} = 0.34$ nm in the present model, as mentioned above. $\lfloor x \rfloor$ denotes the nearest integer of $x$. The theoretical formula was also verified to remain valid in cases of self-assembly of GNRs with defects only if the joint boundaries formed during self-assembly are nearly perfect.

Of course, self-assembly of GNRs inside a basal CNT has some additional requirements [53]. The width of the GNRs must be at least larger than and should not be larger than $W_{cr} = D - 2\sigma$, where $D$ is the diameter of the basal CNT and $\sigma = 0.34$ nm is the equilibrium distance between two non-bonded carbon atoms. If the width of GNRs is larger than $W_{cr}$ but smaller than $D$, helical structures can still be self-assembled inside the basal CNT but with greater difficulty due to the self-adjustment of GNRs by bending or twisting. All GNRs with or without defects in the present study meet the general requirements given above.

### 3.2 Self-assembly of GNRs with arbitrarily distributed defects

The same technique as that used for perfect GNRs was adopted for the self-assembly of GNRs with defects and dopants distributed arbitrarily. When a small part

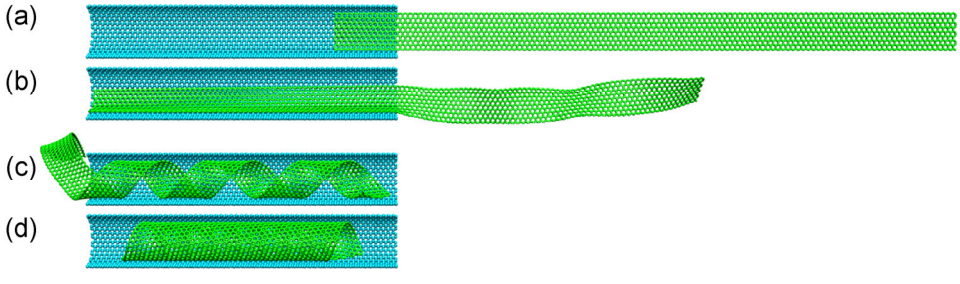


**Figure 2** Snapshot of the self-assembly process of a perfect GNR inside a basal CNT (See Movie S1 in the Electronic Supplementary Material (ESM)).

(forepart) of the defective or doped GNRs is inserted in the basal CNT, GNRs will spontaneously enter the basal CNT very quickly. Because the entire GNR is nearly symmetric in the basal CNT, even in cases with GNRs longer than the basal CNT, GNRs start to curl inside the basal CNT, forming helical structures. The helical structure further converts to self-assembled CNTs with the help of increased temperature. Typical snapshots are shown in Fig. 3(a) for the self-assembly of GNRs with 1.0 at.% of vacancies inside a basal CNT. The initial state is denoted as $t_0$. The intermediate states correspond to snapshots $t_1$ to $t_3$. The final self-assembled configuration is given in snapshot $t_4$, where a CNT forms inside the basal CNT. Similar self-assembly processes are also found for GNRs with arbitrarily distributed SW defects or dopants of boron and nitrogen atoms, and the ultimately self-assembled CNTs are shown in Fig. 3(b) for (i) 1.0 at.% of SW defects; (ii) 1.0 at.% of boron dopants, and (iii) 1.0 at.% of nitrogen dopants.

In order to verify whether C–C bonds formed at the contact neighboring edges shown in Fig. 3, variations in the potential energies of four representative atoms A, B, C, and D are further checked in Fig. 4. Locations of the four atoms are labeled in the inset of Fig. 4. The edge atom C and the inner atom D possess saturated bonds in contrast to atoms A and B, both of which have unsaturated bonds at the unpassivated GNR edges. After sufficient relaxation time, the potential energies of atoms A and B are reduced and finally almost identical to those of atoms C and D, which can be found in Figs. 4(b)–4(d). A small difference in the potential energy exists between atom A (B) and atom C (D), as shown in Fig. 4(a), which is due to the arbitrarily distributed defects located exactly at the edge, leading to an imperfect joint. For a perfect joint, as shown in Figs. 4(b)–4(d), the reduced potential energy of atoms A and B is about a half of the formation energy of a C–C bond, 2.4 eV [45]. All these observations prove that single-walled CNTs can be self-assembled by GNRs with arbitrarily distributed defects or dopants inside a basal CNT.

Geometrical analysis showed that the chirality of the final self-assembled CNT remained (17,9), agreeing well with our theoretical prediction, only if arbitrarily distributed defects were not located at the initial edge

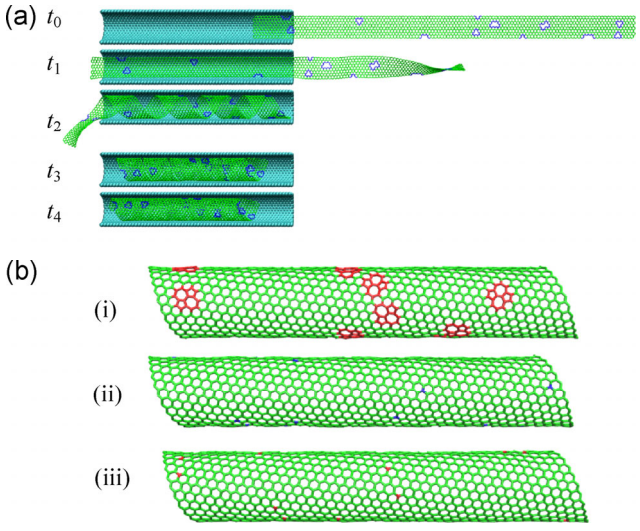


**Figure 3** Snapshot of the self-assembly process of GNRs with arbitrarily distributed defects or dopants. (a) GNRs with vacancies. (b) Final self-assembly structures of GNRs with (i) SW defects, (ii) boron dopants, and (iii) nitrogen dopants. Defects and dopants are labeled with different colors. (See Movies S2–S5 in the ESM.)

of the GNRs and a perfect joint occurred.

The properties of the GNRs, such as the bending stiffness, will change significantly, if the defect fraction in GNRs is too large [54]. Does it influence the self-assembly of GNRs? Further simulations were performed, in which the self-assembly of GNRs with relatively large defect fractions did not work. GNRs may adhere to the outside surface of the basal CNT due to the dramatically decreased bending stiffness of GNRs, leading to arbitrary self-folding. Examples are given in Figs. 5(a) and 5(b) for GNRs with 13.0 at.% of vacancy defects and 5.4 at.% of SW defects, respectively. With SW defects, another underlying mechanism may be the atomic under-coordination effect [54], which induces large in-plane stresses around SW defects, leading to spontaneous inflation [55] and even self-folding [56]. As mentioned above, fractions of either boron or nitrogen dopants are not larger than 9.0 at.% in GNRs in the present work. All GNRs with randomly distributed dopants can be transformed into self-assembled CNTs.

### 3.3 Self-assembly of GNRs with regularly distributed defects

Inspired by the studies above, we further analyzed the possibility and influence factors of self-assembly

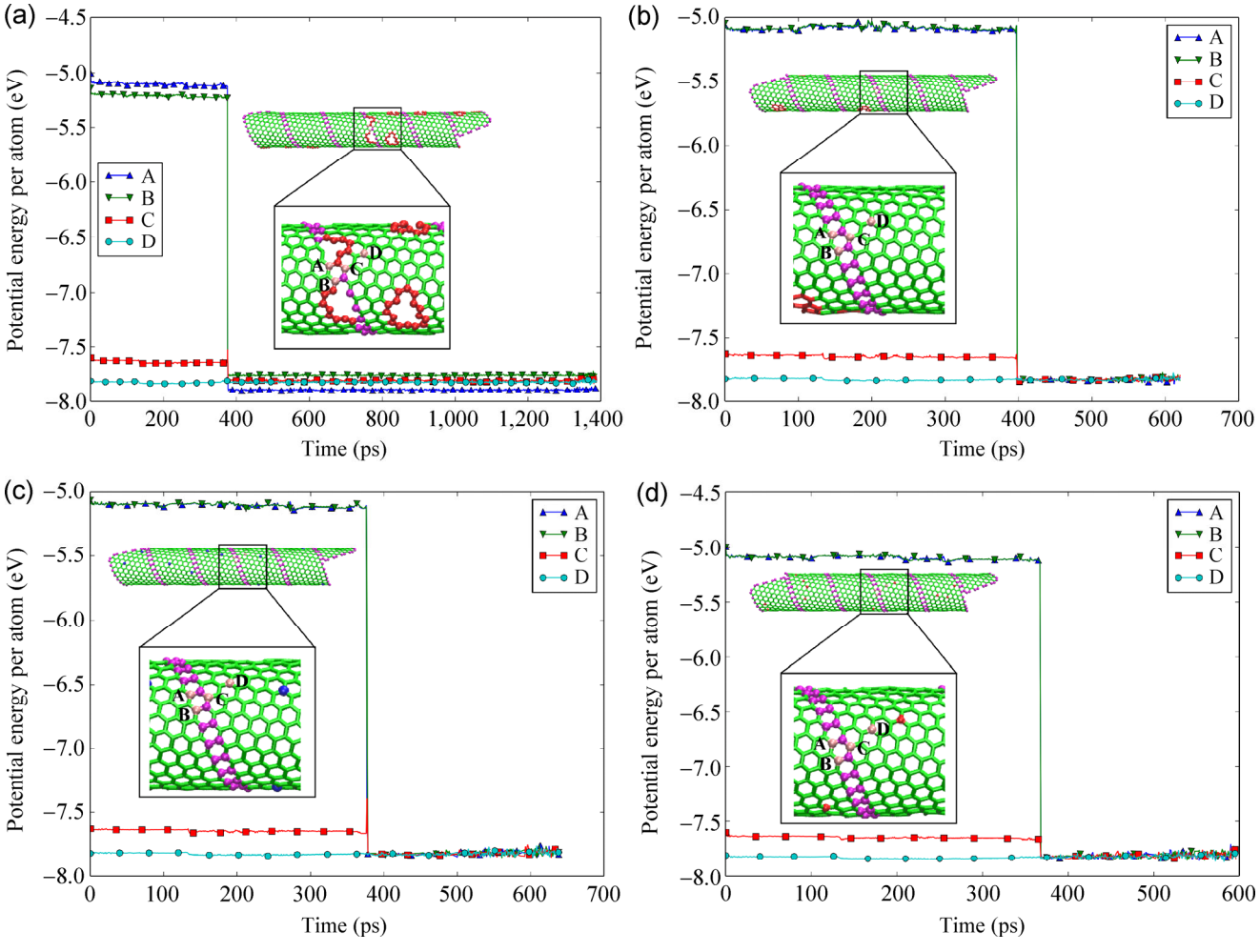


**Figure 4** Variation of the potential energy of four representative atoms in the self-assembly process. (a) Vacancy defects, (b) SW defects, (c) boron dopants, and (d) nitrogen dopants. The positions of atoms A, B, C, and D are labeled in the inset.

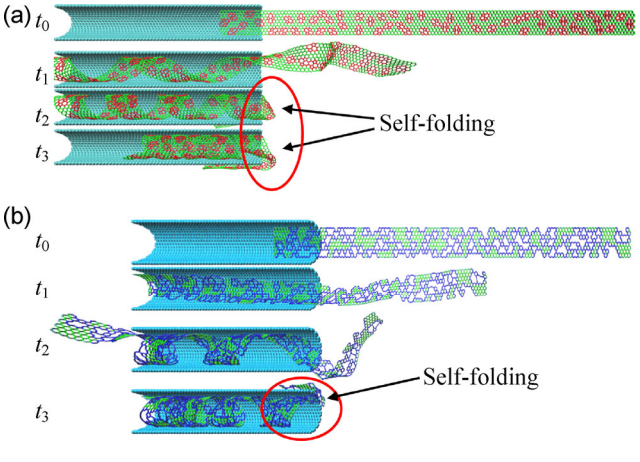


**Figure 5** Self-folding during the self-assembly of GNRs with relatively large defect fractions. (a) 13.0 at.% of vacancies; (b) 5.4 at.% of SW defects.

of GNRs with regularly distributed defects or dopants in order to find a way to fabricate defect- or dopant-controlled CNTs. All the techniques were similar to the former cases except that defects and dopants were distributed regularly in GNRs. Several types of defect-distributing forms were considered, and it was found that all GNRs can self-assemble into CNTs only if the defect fraction is not too large. Otherwise, GNRs will self-fold, and disordered structures will form eventually. Examples are shown in Fig. 6(a), where the initial state of GNRs with (i) a single monovacancy, (ii) a single divacancy, (iii) a line of monovacancies with an inter-distance of 1.476 nm, (iv) two lines of monovacancies with an inter-distance of 1.472 nm in the direction of the GNR length and 0.672 nm along the GNR width, (v) a line of divacancies

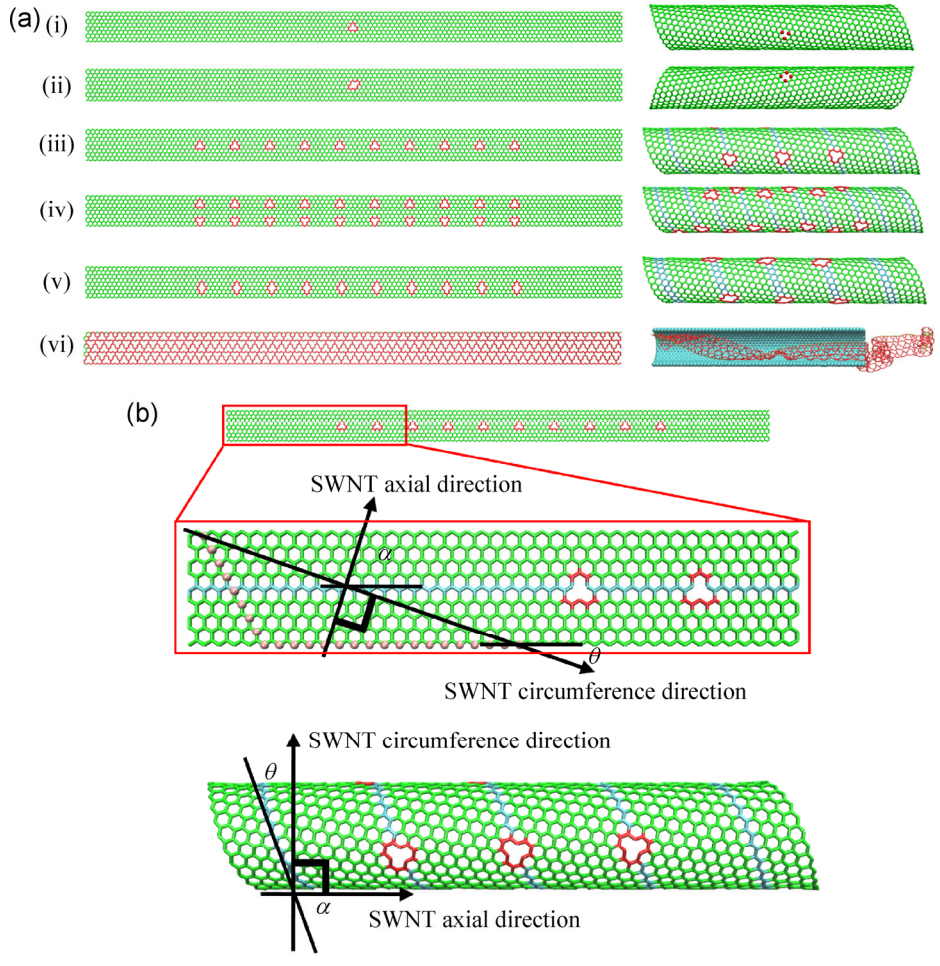


**Figure 6** Comparison of the initial GNRs and the final self-assembled structures. (a) The configuration of initial GNRs with regularly distributed vacancy defects and that of self-assembled CNTs or disordered structures: (i) a single monovacancy, (ii) a single divacancy, (iii) a line of monovacancies, (iv) two lines of monovacancies, (v) a line of divacancies, (vi) a relatively large fraction of defects. (b) Schematic of the geometric mapping between the initial GNR and the final CNT.

with an inter-distance of 1.472 nm, which is shown in the left column, and (vi) a defect fraction in GNRs of nearly 13.6 at.%. The final self-assembled CNTs and disordered structures are shown in the right column. The location of defects in self-assembled CNTs could be predicted by geometric mapping since the distribution of defects in GNRs was regular and known a priori. An example is shown in Fig. 6(b), which corresponds to case (iii). The initial location of vacancies in GNRs was parallel to its long edges. An angle $\theta$ between the circumference of the self-assembled CNT and the long edge of GNRs was predicted to be 19.9°. As a result, the angle $\alpha$ between the direction of the vacancy array and that of the self-assembled CNT axis was 70.1°.

Figure 7 shows five representative examples with regularly distributed Stone-Wales defects. The initial state of GNRs with (a) a single SW defect, (b) two SW defects, (c) a line of 20 SW defects with an inter-distance of 1.47 nm, (d) a line of 30 SW defects with an inter-distance of 0.492 nm, and (e) a line of 40 SW defects with an inter-distance of 0.246 nm is shown in the left column of Fig. 7 with the corresponding final self-assembled configurations in the right column. It is very obvious that CNTs can be self-assembled in cases with relatively small SW defect fractions, while self-folding structures form in cases with relatively large SW defect fractions. The reasons for the two different results should be the same as those in previous cases with arbitrarily distributed SW defects.

However, the bending stiffness of GNRs with distributed dopants will not vary much and should not influence the self-assembly process very obviously. Actually, it was found that all GNRs with regularly distributed dopants could be self-assembled into CNTs, very similar to cases with arbitrarily distributed dopants or without dopants, though only cases with dopant fractions not larger than 9.0 at.% were considered. Some representative examples are shown in Fig. 8, where the left column denotes initial states with (a) one boron dopant, (b) one nitrogen dopant, (c) a pair of boron-nitrogen dopants, (d) a line of boron dopants, (e) a line of nitrogen dopants, (f) two lines of boron dopants, and (g) two lines of nitrogen dopants, and the right column shows the corresponding self-assembled CNTs, respectively.

All the above simulations demonstrate the possibility of the fabrication of defect- or dopant-controlled CNTs through the self-assembly technique of GNRs with regularly distributed defects or dopants. Furthermore, the locations of distributed defects or dopants in self-assembled CNTs can be designed by tuning the basal CNT radius, the width of the GNRs, and the initial distribution of defects or dopants in the GNRs.

### 3.4 Effect of temperature on the self-assembly of GNRs

As emphasized above, the technique of increasing the temperature was adopted directly in the present study. The motivation was to fabricate self-assembled CNTs with as few defects as possible emerging at joint boundaries. Here, some typical self-assembled

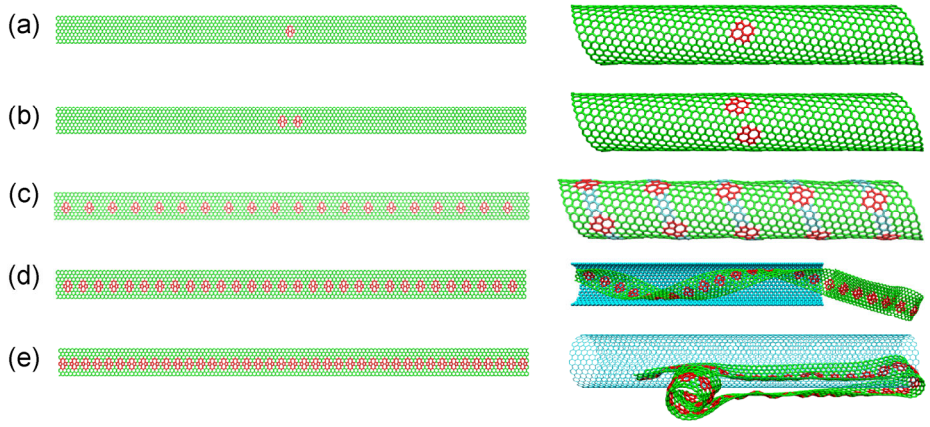


**Figure 7** The initial configuration of GNRs with regularly distributed SW defects and the final configuration of self-assembled structures: (a) single SW defect, (b) two SW defects, (c) a line of 20 SW defects, (d) a line of 30 SW defects, and (e) a line of 40 SW defects.

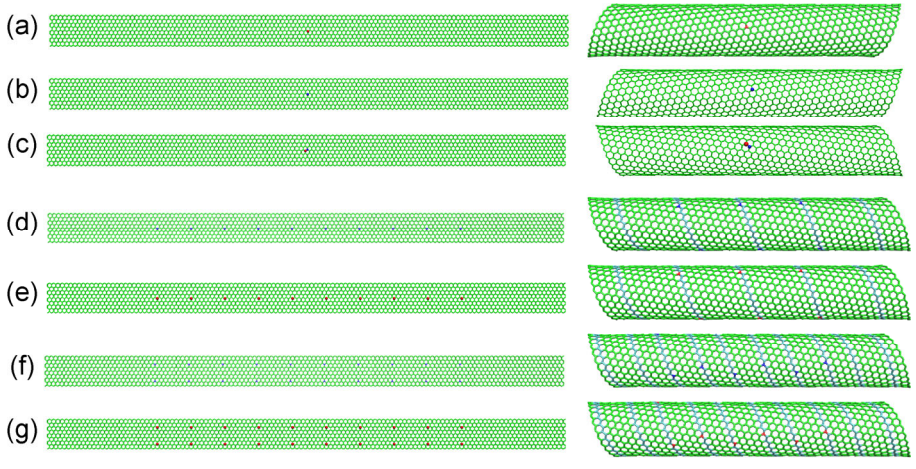


**Figure 8** The initial configuration of GNRs with regularly distributed dopants and the final configuration of self-assembled CNTs. (a) One boron dopant, (b) one nitrogen dopant, (c) a pair of boron-nitrogen dopants, (d) a line of boron dopants, (e) a line of nitrogen dopants, (f) two lines of boron dopants, and (g) two lines of nitrogen dopants.

structures are further described for intuitive understanding.

Inspired by our former work [27], we performed a series of simulations at different relatively low or high constant temperatures, for instance, $T$ = 10 and 1,000 K. In essence, self-assembly of GNRs is mainly due to the unavoidable collision of atoms on different parts of edges of GNRs, and the speed at which the edges travel depends significantly on the system temperature. At a relatively low temperature, for example, 10 K, GNRs can invariably self-assemble into helical structures but not always into nanotubes. However, if the temperature is relatively high, for example, 1,000 K, the edges of GNRs will move very quickly, and flaws during the process of forming C–C bonds at the joint edges cannot be avoided because there is insufficient time for the edges of GNRs to wrap themselves around the basal CNT. Figure 9 gives the final self-assembled CNTs at constant temperatures of 10 and 1,000 K, where flaws can be found easily at the joint edges.

## 4 Conclusion

Reactive molecular dynamics simulations were performed in order to determine whether self-assembly of GNRs inside a basal CNT can lead to the fabrication of defect- or dopant-controlled CNTs. The technique of increasing the temperature was adopted in our simulation. Both arbitrarily distributed defects and regularly distributed defects were investigated. It was found that the defect fraction in GNRs is the main factor that influences the success of self-assembled CNTs. In cases with relatively small defect fractions, CNTs can be easily fabricated. Otherwise, the self-assembly of CNTs fails mainly because of the mechanical strength, which is influenced by the atomic under-coordination effect [54]. Defect-controlled CNTs can be obtained with regularly distributed defects in GNRs. Several cases of dopants in GNRs were further considered. With the same method, dopant-controlled CNTs can be easily achieved as well. The finding reported here should be very helpful not only for the fabrication of carbon nanotubes with metallic or semi-conductive properties but also for the design of carbon nanotubes with electromagnetic induction characteristics.

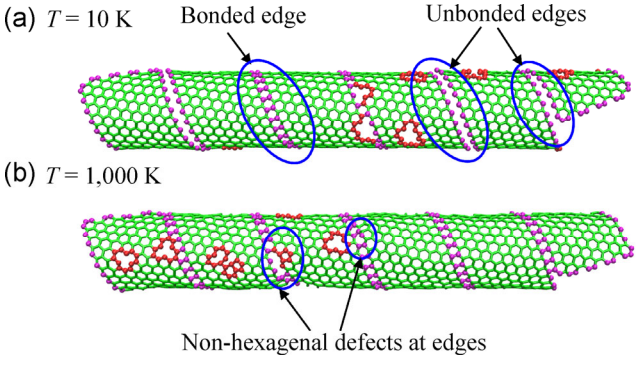


**Figure 9** The effect of temperature on the self-assembly of GNRs with 1.0 at.% of arbitrarily distributed vacancy defects (a) at $T$ = 10 K and (b) at $T$ = 1,000 K.

## Acknowledgements

The work reported here is supported by the National Natural Science Foundation of China (Nos. 11125211 and 11372317), and the National Basic Research Program of China (No. 2012CB937500). MD simulations are carried out at Supercomputing Center of Chinese Academy of Sciences.

**Electronic Supplementary Material**: Supplementary material (movies related to the self-assembly of graphene nanoribbons) is available in the online version of this article at http://dx.doi.org/10.1007/s12274-015-0804-0.

## References

[1] Charlier, J.-C. Defects in carbon nanotubes. *Acc. Chem. Res.* **2002**, *35*, 1063–1069.

[2] Jana, D.; Sun, C.-L.; Chen, L.-C.; Chen, K.-H. Effect of chemical doping of boron and nitrogen on the electronic, optical, and electrochemical properties of carbon nanotubes. *Prog. Mater. Sci.* **2013**, *58*, 565–635.

[3] Terrones, H.; Lv, R. T.; Terrones, M.; Dresselhaus, M. S. The role of defects and doping in 2D graphene sheets and 1D nanoribbons. *Rep. Prog. Phys.* **2012**, *75*, 062501.

[4] Yeung, C. S.; Chen, Y. K.; Wang, Y. A. Defected and substitutionally doped nanotubes: Applications in biosystems, sensors, nanoelectronics, and catalysis. In *Carbon Nanotubes—Growth and Applications*; Naraghi, M., Ed.; InTech: Croatia, 2011; pp 97–132.

[5] Zhou, Q.-X.; Wang, C.-Y.; Fu, Z.-B.; Tang, Y.-J.; Zhang, H. Effects of various defects on the electronic properties of

single-walled carbon nanotubes: A first principle study. *Front. Phys.* **2014**, *9*, 200–209.

[6] Zeng, H.; Zhao, J.; Hu, H. F.; Leburton, J.-P. Atomic vacancy defects in the electronic properties of semi-metallic carbon nanotubes. *J. Appl. Phys.* **2011**, *109*, 83716–83716.

[7] Rodríguez-Manzo, J. A.; Cretu, O.; Banhart, F. Trapping of metal atoms in vacancies of carbon nanotubes and graphene. *ACS Nano* **2010**, *4*, 3422–3428.

[8] Choi, H.; Ihm, J.; Louie, S.; Cohen, M. Defects, quasibound states, and quantum conductance in metallic carbon nanotubes. *Phys. Rev. Lett.* **2000**, *84*, 2917–2920.

[9] Lü, X. L.; Yu, G. D.; Yao, H. B.; Zheng, Y. S. A valley-filtering switch based on the stone-wales defect array in carbon nanotube. *EPL-Europhys. Lett.* **2013**, *103*, 47008–47008.

[10] Carroll, D. L.; Redlich, P.; Blase, X.; Charlier, J.-C.; Curran, S.; Ajayan, P. M.; Roth, S.; Rühle, M. Effects of nanodomain formation on the electronic structure of doped carbon nanotubes. *Phys. Rev. Lett.* **1998**, *81*, 2332–2335.

[11] Czerw, R.; Terrones, M.; Charlier, J.-C.; Blase, X.; Foley, B.; Kamalakaran, R.; Grobert, N.; Terrones, H.; Tekleab, D.; Ajayan, P. M. et al. Identification of electron donor states in N-doped carbon nanotubes. *Nano Lett.* **2001**, *1*, 457–460.

[12] Xu, Z.; Lu, W. G.; Wang, W. L.; Gu, C. Z.; Liu, K. H.; Bai, X. D.; Wang, E. G.; Dai, H. J. Converting metallic single-walled carbon nanotubes into semiconductors by boron/nitrogen co-doping. *Adv. Mater.* **2008**, *20*, 3615–3619.

[13] Zhang, Z.-Y.; Miao, C. Y.; Guo, W. L. Nano-solenoid: Helicoid carbon-boron nitride hetero-nanotube. *Nanoscale* **2013**, *5*, 11902–11909.

[14] Du, A. J.; Chen, Y.; Zhu, Z. H.; Lu, G. Q.; Smith, S. C. C-BN single-walled nanotubes from hybrid connection of BN/C nanoribbons: Prediction by *ab initio* density functional calculations. *J. Am. Chem. Soc.* **2009**, *131*, 1682–1683.

[15] Audiffred, M.; Elías, A. L.; Gutiérrez, H. R.; López-Urías, F.; Terrones, H.; Merino, G.; Terrones, M. Nitrogen–silicon heterodoping of carbon nanotubes. *J. Phys. Chem. C* **2013**, *117*, 8481–8490.

[16] Ayala, P.; Plank, W.; Grüneis, A.; Kauppinen, E. I.; Rümmeli, M. H.; Kuzmany, H.; Pichler, T. A one step approach to B-doped single-walled carbon nanotubes. *J. Mater. Chem.* **2008**, *18*, 5676–5681.

[17] Blackburn, J. L.; Yan, Y. F.; Engtrakul, C.; Parilla, P. A.; Jones, K.; Gennett, T.; Dillon, A. C.; Heben, M. J. Synthesis and characterization of boron-doped single-wall carbon nanotubes produced by the laser vaporization technique. *Chem. Mater.* **2006**, *18*, 2558–2566.

[18] Wu, M.-H.; Li, X.; Pan, D.; Liu, L.; Yang, X.-X.; Xu, Z.; Wang, W.-L.; Sui, Y.; Bai, X.-D. Synthesis of nitrogen-doped single-walled carbon nanotubes and monitoring of doping by Raman spectroscopy. *Chin. Phys. B* **2013**, *22*, 086101.

[19] Balasubramanian, K.; Burghard, M. Chemically functionalized carbon nanotubes. *Small* **2005**, *1*, 180–192.

[20] Borowiak-Palen, E.; Pichler, T.; Fuentes, G. G.; Graff, A.; Kalenczuk, R. J.; Knupfer, M.; Fink, J. Efficient production of B-substituted single-wall carbon nanotubes. *Chem. Phys. Lett.* **2003**, *378*, 516–520.

[21] Borowiak-Palen, E.; Pichler, T.; Graff, A.; Kalenczuk, R. J.; Knupfer, M.; Fink, J. Synthesis and electronic properties of B-doped single wall carbon nanotubes. *Carbon* **2004**, *42*, 1123–1126.

[22] Golberg, D.; Bando, Y.; Bourgeois, L.; Kurashima, K.; Sato, T. Large-scale synthesis and HRTEM analysis of single-walled B-and N-doped carbon nanotube bundles. *Carbon* **2000**, *38*, 2017–2027.

[23] Han, W. Q.; Bando, Y.; Kurashima, K.; Sato, T. Boron-doped carbon nanotubes prepared through a substitution reaction. *Chem. Phys. Lett.* **1999**, *299*, 368–373.

[24] Zhang, Y. X.; Zhang, J.; Su, D. S. Substitutional doping of carbon nanotubes with heteroatoms and their chemical applications. *ChemSusChem* **2014**, *7*, 1240–1250.

[25] Rodriguez-Manzo, J. A.; Banhart, F. Creation of individual vacancies in carbon nanotubes by using an electron beam of 1 Å diameter. *Nano Lett.* **2009**, *9*, 2285–2289.

[26] Lim, H. E.; Miyata, Y.; Kitaura, R.; Nishimura, Y.; Nishimoto, Y.; Irle, S.; Warner, J. H.; Kataura, H.; Shinohara, H. Growth of carbon nanotubes via twisted graphene nanoribbons. *Nat. Commun.* **2013**, *4*, 2548.

[27] Zhang, C.; Peng, Z. L.; Chen, S. H. Chirality-controlled carbon nanotubes fabricated by self-assembly of graphene nanoribbons. *J. Phys. Chem. C* **2014**, *118*, 19477–19483.

[28] Banhart, F.; Kotakoski, J.; Krasheninnikov, A. V. Structural defects in graphene. *ACS Nano* **2011**, *5*, 26–41.

[29] Yang, B.; Boscoboinik, J. A.; Yu, X.; Shaikhutdinov, S.; Freund, H.-J. Patterned defect structures predicted for graphene are observed on single-layer silica films. *Nano Lett.* **2013**, *13*, 4422–4427.

[30] Cai, J. M.; Ruffieux, P.; Jaafar, R.; Bieri, M.; Braun, T.; Blankenburg, S.; Muoth, M.; Seitsonen, A. P.; Saleh, M.; Feng, X. L. et al. Atomically precise bottom-up fabrication of graphene nanoribbons. *Nature* **2010**, *466*, 470–473.

[31] Wang, H. T.; Wang, Q. X.; Cheng, Y. C.; Li, K.; Yao, Y. B.; Zhang, Q.; Dong, C. Z.; Wang, P.; Schwingenschlögl, U.; Yang, W. et al. Doping monolayer graphene with single atom substitutions. *Nano Lett.* **2012**, *12*, 141–144.

[32] Lahiri, J.; Lin, Y.; Bozkurt, P.; Oleynik, I. I.; Batzill, M. An extended defect in graphene as a metallic wire. *Nat. Nanotechnol.* **2010**, *5*, 326–329.

[33] Liu, Z.; Ma, L. L.; Shi, G.; Zhou, W.; Gong, Y. J.; Lei, S. D.; Yang, X. B.; Zhang, J. N.; Yu, J. J.; Hackenberg, K. P. et al. In-plane heterostructures of graphene and hexagonal boron nitride with controlled domain sizes. *Nat. Nanotechnol.* **2013**, *8*, 119–124.

[34] Robertson, A. W.; Allen, C. S.; Wu, Y. A.; He, K.; Olivier, J.; Neethling, J.; Kirkland, A. I.; Warner, J. H. Spatial control of defect creation in graphene at the nanoscale. *Nat. Commun.* **2012**, *3*, 1144.

[35] Börrnert, F.; Fu, L.; Gorantla, S.; Knupfer, M.; Büchner, B.; Rümmeli, M. H. Programmable sub-nanometer sculpting of graphene with electron beams. *ACS Nano* **2012**, *6*, 10327–10334.

[36] Chamberlain, T. W.; Biskupek, J.; Rance, G. A.; Chuvilin, A.; Alexander, T. J.; Bichoutskaia, E.; Kaiser, U.; Khlobystov, A. N. Size, structure, and helical twist of graphene nanoribbons controlled by confinement in carbon nanotubes. *ACS Nano* **2012**, *6*, 3943–3953.

[37] Jiao, L. Y.; Zhang, L.; Wang, X. R.; Diankov, G.; Dai, H. J. Narrow graphene nanoribbons from carbon nanotubes. *Nature* **2009**, *458*, 877–880.

[38] Kosynkin, D. V.; Higginbotham, A. L.; Sinitskii, A.; Lomeda, J. R.; Dimiev, A.; Price, B. K.; Tour, J. M. Longitudinal unzipping of carbon nanotubes to form graphene nanoribbons. *Nature* **2009**, *458*, 872–876.

[39] Han, M. Y.; Özyilmaz, B.; Zhang, Y. B.; Kim, P. Energy band-gap engineering of graphene nanoribbons. *Phys. Rev. Lett.* **2007**, *98*, 206805.

[40] Tapasztó, L.; Dobrik, G.; Lambin, P.; Biró, L. P. Tailoring the atomic structure of graphene nanoribbons by scanning tunnelling microscope lithography. *Nat. Nanotechnol.* **2008**, *3*, 397–401.

[41] Huang, Q. S.; Kim, J. J.; Ali, G.; Cho, S. O. Width-tunable graphene nanoribbons on a SiC substrate with a controlled step height. *Adv. Mater.* **2013**, *25*, 1144–1148.

[42] Sprinkle, M.; Ruan, M.; Hu, Y.; Hankinson, J.; Rubio-Roy, M.; Zhang, B.; Wu, X.; Berger, C.; de Heer, W. A. Scalable templated growth of graphene nanoribbons on SiC. *Nat. Nanotechnol.* **2010**, *5*, 727–731.

[43] Campos-Delgado, J.; Romo-Herrera, J. M.; Jia, X. T.; Cullen, D. A.; Muramatsu, H.; Kim, Y. A.; Hayashi, T.; Ren, Z. F.; Smith, D. J.; Okuno, Y. et al. Bulk production of a new form of $sp^2$ carbon: Crystalline graphene nanoribbons. *Nano Lett.* **2008**, *8*, 2773–2778.

[44] Ma, L.; Wang, J. L.; Ding, F. Recent progress and challenges in graphene nanoribbon synthesis. *ChemPhysChem* **2013**, *14*, 47–54.

[45] Stuart, S. J.; Tutein, A. B.; Harrison, J. A. A reactive potential for hydrocarbons with intermolecular interactions. *J. Chem. Phys.* **2000**, *112*, 6472–6486.

[46] Kınacı, A.; Haskins, J. B.; Sevik, C.; Çağın, T. Thermal conductivity of BN-C nanostructures. *Phys. Rev. B* **2012**, *86*, 115410.

[47] Brenner, D. W.; Shenderova, O. A.; Harrison, J. A.; Stuart, S. J.; Ni, B.; Sinnott, S. B. A second-generation reactive empirical bond order (REBO) potential energy expression for hydrocarbons. *J. Phys.-Condens. Matter* **2002**, *14*, 783–802.

[48] Thamwattana, N.; Hill, J. M. Continuum modelling for carbon and boron nitride nanostructures. *J. Phys.-Condens. Matter* **2007**, *19*, 406209.

[49] Plimpton, S. Fast parallel algorithms for short-range molecular dynamics. *J. Comp. Phys.* **1995**, *117*, 1–19.

[50] Evans, D. J.; Holian, B. L. The Nose–Hoover thermostat. *J. Chem. Phys.* **1985**, *83*, 4069–4074.

[51] Humphrey, W.; Dalke, A.; Schulten, K. VMD: Visual molecular dynamics. *J. Mol. Graph.* **1996**, *14*, 33–38.

[52] Chuvilin, A.; Bichoutskaia, E.; Gimenez-Lopez, M. C.; Chamberlain, T. W.; Rance, G. A.; Kuganathan, N.; Biskupek, J.; Kaiser, U.; Khlobystov, A. N. Self-assembly of a sulphur-terminated graphene nanoribbon within a single-walled carbon nanotube. *Nat. Mater.* **2011**, *10*, 687–692.

[53] Li, Y. F.; Sun, F. W.; Li, H. Helical wrapping and insertion of graphene nanoribbon to single-walled carbon nanotube. *J. Phys. Chem. C* **2011**, *115*, 18459–18467.

[54] Sun, C. Q. Thermo-mechanical behavior of low-dimensional systems: The local bond average approach. *Prog. Mater. Sci.* **2009**, *54*, 179–307.

[55] Zhang, J. F.; Zhao, J. J.; Lu, J. P. Intrinsic strength and failure behaviors of graphene grain boundaries. *ACS Nano* **2012**, *6*, 2704–2711.

[56] Sgouros, A.; Sigalas, M. M.; Papagelis, K.; Kalosakas, G. Transforming graphene nanoribbons into nanotubes by use of point defects. *J. Phys.-Condens. Matter* **2014**, *26*, 125301.